
Training Quantized Nets: A Deeper Understanding

Hao Li^{1*}, Soham De^{1*}, Zheng Xu¹, Christoph Studer², Hanan Samet¹, Tom Goldstein¹

¹Department of Computer Science, University of Maryland, College Park

²School of Electrical and Computer Engineering, Cornell University

{haoli, sohamde, xuzh, hjs, tomg}@cs.umd.edu, studer@cornell.edu

Abstract

Currently, deep neural networks are deployed on low-power embedded devices by first training a full-precision model using powerful computing hardware, and then deriving a corresponding low-precision model for efficient inference on such systems. However, training models directly with coarsely quantized weights is a key step towards learning on embedded platforms that have limited computing resources, memory capacity, and power consumption. Numerous recent publications have studied methods for training quantized network, but these studies have mostly been empirical. In this work, we investigate training methods for quantized neural networks from a theoretical viewpoint. We first explore accuracy guarantees for training methods under convexity assumptions. We then look at the behavior of algorithms for non-convex problems, and we show that training algorithms that exploit high-precision representations have an important annealing property that purely quantized training methods lack, which explains many of the observed empirical differences between these types of algorithms.

1 Introduction

Deep neural networks (NNs) are an integral part of numerous state-of-the-art computer vision and natural language processing tasks. The networks are usually designed and trained using powerful hardware because of their high memory requirements and computational complexity. There is an increasing interest in training and deploying neural networks directly on battery-powered devices, such as cell phones or other platforms. Such low-power embedded systems are, however, memory and power limited, and in some cases lack basic support for floating-point arithmetic.

To make neural nets practical on embedded systems, many researchers have focused on training nets with *coarsely quantized* weights. For example, weights may be constrained to take on integer/binary values, or may be represented using low-precision (8 bits or less) fixed-point numbers. Quantized nets offer superior memory and computation efficiency, while achieving a performance that is competitive with state-of-the-art high-precision nets. Quantized weights can dramatically reduce memory size and access bandwidth, increase power efficiency [1], exploit hardware-friendly bitwise operations [2], and accelerate inference throughput [3, 4].

Despite these benefits, handling coarsely quantized weights is, in general, difficult and motivates interest in new training methods. The naive approach of quantizing pre-trained weights using a rounding procedure yields poor results when weights are represented using a small number of bits. Other approaches include classical stochastic rounding methods [5], as well as schemes that combine full-precision floating-point weights with discrete rounding procedures [3]. While some of these schemes seem to work in practice, results in this area are largely experimental, and little work has been devoted to explaining the excellent performance of successful methods, as well as the important differences in behavior between these methods, from a principled mathematical perspective.

Contributions This paper studies quantized training methods from a theoretical perspective, with the goal of understanding the differences in behavior, and reasons for success or failure, of various

*Equal contribution. Author ordering determined by coin flip.

methods. In particular, we present a convergence analysis showing that both the classical stochastic rounding (SR) methods [5] as well as newer and more powerful methods like BinaryConnect (BC) [3] are capable of solving convex discrete problems up to a level of accuracy that depends on the quantization level. We then address the issue of why algorithms that maintain floating-point representations, like BC, work so well, while fully quantized training methods like SR stall before training is complete. We show that the long-term behavior of BC has an important annealing property that is needed for non-convex optimization, while classical rounding methods lack this property.

2 Background and Related Work

The arithmetic operations of deep networks can be encoded down to 8-bit fixed-point without significant deterioration in inference performance [5–9]. The most extreme scenario of quantization is binarization, in which only 1-bit (two states) is available for weight representation [10, 3, 1, 4, 11, 12].

Previous work on obtaining a quantized neural network (NN) can be divided into two categories: quantizing pre-trained models with or without retraining [7, 13, 6, 14, 15], and training a quantized model from scratch [5, 3, 4, 1, 16]. We focus on approaches that belong to the second category, as they can be used for both training and inference under constrained resources.

For training quantized NNs from scratch, many authors suggest maintaining a high-precision copy of the weights while feeding quantized weights into backprop [3, 11, 4, 16], which results in good empirical performance. There are limitations in using such methods on low-power devices, however, where floating-point arithmetic is not available or not desirable. Another widely used solution using only low-precision weights is *stochastic rounding* [17, 5]. Experiments show that networks using 16-bit fixed-point representations with stochastic rounding can deliver results nearly identical to 32-bit floating-point computations [5], while lowering the precision down to 3-bit fixed-point often results in a significant performance degradation [18]. Bayesian learning has also been applied to train binary networks [19, 20]. A more comprehensive review can be found in [4].

3 Training Quantized Neural Nets

We consider empirical risk minimization problems of the form:

$$\min_{w \in \mathcal{W}} F(w) := \frac{1}{m} \sum_{i=1}^m f_i(w), \quad (1)$$

where the objective function decomposes into a sum over many functions $f_i : \mathbb{R}^d \rightarrow \mathbb{R}$. Neural networks have objective functions of this form where each f_i is a non-convex loss function. When floating-point representations are available, the standard method for training neural networks is stochastic gradient descent (SGD), which on each iteration selects a function \tilde{f} randomly from $\{f_1, f_2, \dots, f_m\}$, and then computes

$$\text{SGD: } w^{t+1} = w^t - \alpha_t \nabla \tilde{f}(w^t), \quad (2)$$

for some learning rate α_t . In this paper, we consider the problem of training convolutional neural networks (CNNs). In CNNs, each convolutional layer i accepts inputs x_i and generates the response corresponding to filter j with linear transformation $a_{i,j} = w_{i,j} * x_i + b_j$, where $w_{i,j}$ represent the vector of weights of filter j at layer i , and $*$ denotes the convolution operation. The neuron output is generated by applying a non-linear activation function $h(\cdot)$ to the filter response, i.e., $x_{i+1} = h(a_i)$, which is used as the input to the next layer. Convolutions are expensive; low precision weights can be used to accelerate the convolutions by replacing expensive multiplications with binary operations or dedicated high-performance computer arithmetic.

To train neural networks using a low-precision representation of the weights, a quantization function $Q(\cdot)$ is required that converts a real-valued number w into a quantized version $\hat{w} = Q(w)$. We use the same notation for quantizing vectors, where we assume Q acts on each dimension of the vector. Different quantized optimization routines can be defined by selecting different quantizers, and also by selecting when quantization happens during optimization. The common options are:

Deterministic Rounding (R) A basic *uniform* or deterministic quantization function converts a floating point value to the closest quantized value as:

$$Q_d(w) = \text{sign}(w) \cdot \Delta \cdot \left\lfloor \frac{|w|}{\Delta} + \frac{1}{2} \right\rfloor \quad (3)$$

where Δ denotes the quantization step or resolution, i.e., the smallest positive number that is representable. One exception to this definition is when we consider binary weights, where all weights are constrained to have two values $w \in \{-1, 1\}$ and uniform rounding becomes $Q_d(w) = \text{sign}(w)$.

The deterministic rounding SGD maintains quantized weights with updates of the form:

$$\text{Deterministic Rounding: } w_b^{t+1} = Q_d(w_b^t - \alpha_t \nabla \tilde{f}(w_b^t)), \quad (4)$$

where w_b denotes the low-precision weights, which are quantized using Q_d immediately after applying the gradient descent update. If gradient updates are significantly smaller than the quantization step, this method loses gradient information and weights may never be modified from their starting values.

Stochastic Rounding (SR) The quantization function for *stochastic rounding* is defined as:

$$Q_s(w) = \Delta \cdot \begin{cases} \lfloor \frac{w}{\Delta} \rfloor + 1 & \text{for } p \leq \frac{w}{\Delta} - \lfloor \frac{w}{\Delta} \rfloor, \\ \lfloor \frac{w}{\Delta} \rfloor & \text{otherwise,} \end{cases} \quad (5)$$

where $p \in [0, 1]$ is produced by a uniform random number generator. This operator is non-deterministic, and rounds its argument up with probability $w/\Delta - \lfloor w/\Delta \rfloor$, and down otherwise. This quantizer satisfies the important property $\mathbb{E}[Q_s(w)] = w$. Similar to the deterministic rounding method, the SR optimization method also maintains quantized weights with updates of the form:

$$\text{Stochastic Rounding: } w_b^{t+1} = Q_s(w_b^t - \alpha_t \nabla \tilde{f}(w_b^t)). \quad (6)$$

BinaryConnect (BC) The BinaryConnect algorithm [3] accumulates gradient updates using a full-precision buffer w_r , and quantizes weights only just before gradient computations. BinaryConnect uses updates of the form:

$$\text{BinaryConnect: } w_r^{t+1} = w_r^t - \alpha_t \nabla \tilde{f}(Q(w_r^t)). \quad (7)$$

Either stochastic rounding Q_s or deterministic rounding Q_d can be used for quantizing the weights w_r , but in practice, Q_d is the common choice. The original BinaryConnect paper constrains the weights to be $\{-1, 1\}$, which can be generalized to $\{-\Delta, \Delta\}$. A more recent method, Binary-Weights-Net (BWN) [4], allows different filters to have different scales for quantization, which often results in better performance on large datasets.

Notation For the rest of the paper, we use Q to denote both Q_s and Q_d unless the situation requires this to be distinguished. We also drop the subscripts on w_r and w_b , and simply write w .

4 Convergence Analysis

We now present convergence guarantees for the Stochastic Rounding (SR) and BinaryConnect (BC) algorithms, with updates of the form (6) and (7), respectively. For the purposes of deriving theoretical guarantees, we assume each f_i in (1) is differentiable and convex, and the domain \mathcal{W} is convex and has dimension d . We consider both the case where F is μ -strongly convex: $\langle \nabla F(w'), w - w' \rangle \leq F(w) - F(w') - \frac{\mu}{2} \|w - w'\|^2$, as well as where F is non-strongly convex. We also assume the (stochastic) gradients are bounded by $\mathbb{E} \|\nabla \tilde{f}(w^t)\|^2 \leq G^2$. Some results below also assume the domain of the problem is finite. In this case, the rounding algorithm clips values that leave the domain. For example, in the binary case, the rounding algorithm never returns a value outside of $\{-1, 1\}$.

4.1 Convergence of Stochastic Rounding (SR)

We can rewrite the update rule (6) as:

$$w^{t+1} = w^t - \alpha_t \nabla \tilde{f}(w^t) + r^t,$$

where $r^t = Q_s(w^t - \alpha_t \nabla \tilde{f}(w^t)) - w^t + \alpha_t \nabla \tilde{f}(w^t)$ denotes the quantization error on the t -th iteration. We want to bound this error in expectation. To this end, we present the following lemma.

Lemma 1. *The error r^t on each iteration can be bounded, in expectation, as:*

$$\mathbb{E}\|r^t\|^2 \leq \sqrt{d}\Delta\alpha_t G.$$

Proofs for all theoretical results are presented in the Appendices. From Lemma 1, we see that the rounding error per step decreases as the learning rate α_t decreases. This is intuitive since the probability of an entry in w^{t+1} differing from w^t is small when the gradient update is small relative to Δ . Using the above lemma, we now present convergence rate results for Stochastic Rounding (SR) in both the strongly-convex case and the non-strongly convex case. Our error estimates are ergodic, i.e., they are in terms of $\bar{w}^T = \frac{1}{T} \sum_{t=1}^T w^t$, the average of the iterates.

Theorem 1. *Assume that F is μ -strongly convex and the learning rates are given by $\alpha_t = \frac{1}{\mu(t+1)}$. Consider the SR algorithm with updates of the form (6). Then, we have:*

$$\mathbb{E}[F(\bar{w}^T) - F(w^*)] \leq \frac{(1 + \log(T+1))G^2}{2\mu T} + \frac{\sqrt{d}\Delta G}{2}.$$

Theorem 2. *Assume the domain has finite diameter D , and learning rates are given by $\alpha_t = \frac{c}{\sqrt{t}}$, for a constant c . Consider the SR algorithm with updates of the form (6). Then, we have:*

$$\mathbb{E}[F(\bar{w}^T) - F(w^*)] \leq \frac{1}{c\sqrt{T}}D^2 + \frac{\sqrt{T+1}}{2T}cG^2 + \frac{\sqrt{d}\Delta G}{2}.$$

Thus, we see that in both cases, SR converges until it reaches an ‘accuracy floor.’ As the quantization becomes more fine grained, our theory predicts that the accuracy of SR approaches that of high-precision floating point at a rate linear in Δ . This extra term caused by the discretization is unavoidable since this method maintains quantized weights.

4.2 Convergence of Binary Connect (BC)

When analyzing the BC algorithm in the strongly convex case, we assume that the Hessian satisfies $\|\nabla^2 F_i(x) - \nabla^2 F_i(y)\| \leq L_2 \|x - y\|$, or equivalently that $\nabla F_i(y) = \nabla F_i(x) + \nabla^2 F_i(x)(y - x) + \delta$ where $\|\delta\| \leq \frac{L_2}{2} \|x - y\|^2$ and $L_2 > 0$. While this is a slightly non-standard assumption, we will see that it enables us to gain better insights into the behavior of the algorithm.

The results here hold for both stochastic and uniform rounding. In this case, the quantization error r does not approach 0 as in SR-SGD. Nonetheless, the effect of this rounding error diminishes with shrinking α_t because α_t multiplies the gradient update, and thus implicitly the rounding error as well.

Theorem 3. *Assume F is L -Lipschitz smooth, the domain has finite diameter D , and learning rates are given by $\alpha_t = \frac{c}{\sqrt{t}}$. Consider the BC-SGD algorithm with updates of the form (7). Then, we have:*

$$\mathbb{E}[F(\bar{w}^T) - F(w^*)] \leq \frac{1}{2c\sqrt{T}}D^2 + \frac{\sqrt{T+1}}{2T}cG^2 + \sqrt{d}\Delta LD.$$

As with SR, BC can only converge up to an error floor. So far this looks a lot like the convergence guarantees for SR. However, things change when we assume strong convexity and bounded Hessian.

Theorem 4. *Assume that F is μ -strongly convex and the learning rates are given by $\alpha_t = \frac{1}{\mu(t+1)}$. Consider the BC algorithm with updates of the form (7). Then we have:*

$$\mathbb{E}[F(\bar{w}^T) - F(w^*)] \leq \frac{(1 + \log(T+1))G^2}{2\mu T} + \frac{DL_2\sqrt{d}\Delta}{2}.$$

Now, the error floor is determined by both Δ and L_2 . Consider a quadratic least-squares problem, $F(w) = \frac{1}{2}\|Aw - b\|^2$. Here, the gradient of F is linear: $\nabla F(w) = Aw - b$, and the Hessian is constant. Thus, $L_2 = 0$ and we get the following corollary.

Corollary 1. *Assume that F is quadratic of the form $F(w) = \frac{1}{2}\|Aw - b\|^2$ and the learning rates are given by $\alpha_t = \frac{1}{\mu(t+1)}$. The BC algorithm with updates of the form (7) yields*

$$\mathbb{E}[F(\bar{w}^T) - F(w^*)] \leq \frac{(1 + \log(T+1))G^2}{2\mu T}.$$

We see that accumulating the real-valued weights in BC allows it to converge to the *true minimizer* of quadratic losses. Furthermore, this suggests that, when the function behaves like a quadratic on the distance scale Δ , one would expect BC to perform fundamentally better than SR.

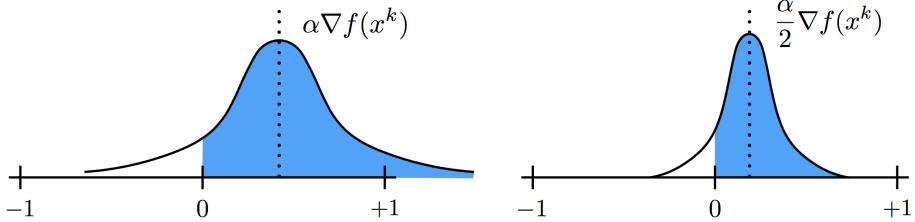


Figure 1: The SR method starts at some location x (in this case 0), adds a perturbation to x , and then rounds. As the learning rate α gets smaller, the distribution of the perturbation gets “squished” near the origin, making the algorithm less likely to move. The “squishing” effect is the same for the part of the distribution lying to the left and to the right of x , and so it does not effect the *relative* probability of moving left or right.

5 What About Non-Convex Problems?

The global convergence results presented above for convex problems show that, in general, both the SR and BC algorithms converge to within $\mathcal{O}(\Delta)$ accuracy of the minimizer (in expected value). However, these results do not explain the large differences in asymptotic behavior between these two methods when applied to non-convex neural nets. We now study the asymptotic, long-term behavior of the SR algorithm as the learning rate gets small. Note that this section makes no convexity assumptions, and the proposed theoretical results are directly applicable to neural networks.

Typical (continuous-valued) SGD methods have an important exploration-exploitation tradeoff. When the learning rate is large, the algorithm explores by moving quickly between states. Exploitation happens when the learning rate is small. In this case, noise averaging causes the algorithm to behave more like deterministic gradient descent, where the algorithm more greedily pursues local minimizers with lower loss function values. Thus, the distribution of iterates produced by the algorithm becomes increasingly concentrated near minimizers as the learning rate vanishes (see, e.g., the large-deviations estimates in [21]). BC maintains this property as well—indeed, we saw in Corollary 1 a class of problems for which the iterates concentrate near the minimizer for small α_t .

In this section, we show that the SR method lacks this important tradeoff: as the stepsize gets small and the algorithm slows down, the quality of the iterates produced by the algorithm does *not* improve, and the algorithm does *not* become progressively more likely to produce low-loss iterates.

To understand this problem conceptually, consider the simplified case of a single-variable optimization problem starting at $x^0 = 0$ with $\Delta = 1$, as depicted in Figure 1. On each iteration, the algorithm computes a stochastic approximation $\nabla \tilde{f}$ of the gradient by sampling from a distribution, which we call p . This gradient is then multiplied by the stepsize to get $\alpha \nabla \tilde{f}$. The probability of moving to the left or right is then roughly proportional to the magnitude of $\alpha \nabla \tilde{f}$. Note that random variable $\alpha \nabla \tilde{f}$ has distribution $p_\alpha(z) = \alpha^{-1} p(z/\alpha)$.

Now, suppose that α is small enough that we can neglect the tails of $p_\alpha(z)$ that lie outside the interval $[-1, 1]$. The probability of transitioning from $x^0 = 0$ to $x^1 = 1$ using stochastic rounding, denoted by $T_\alpha(0, 1)$, is then

$$T_\alpha(0, 1) \approx \int_0^1 z p_\alpha(z) dz = \frac{1}{\alpha} \int_0^1 z p(z/\alpha) dz = \alpha \int_0^{1/\alpha} p(x) x dx \approx \alpha \int_0^\infty p(x) x dx,$$

where the first approximation is because we neglected the unlikely case that $\alpha \nabla \tilde{f} > 1$, and the second approximation appears because we added a small tail probability to the estimate. These approximations get more accurate for small α . We see that, assuming the tails of p are “light” enough, we have $T_\alpha(0, 1) \sim \alpha \int_0^\infty p(x) x dx$ as $\alpha \rightarrow 0$. Similarly, $T_\alpha(0, -1) \sim \alpha \int_{-\infty}^0 p(x) x dx$ as $\alpha \rightarrow 0$.

What does this observation mean for the behavior of SR? First of all, the probability of leaving x^0 on an iteration is

$$T_\alpha(0, -1) + T_\alpha(0, 1) \approx \alpha \left[\int_0^\infty p(x) x dx + \int_{-\infty}^0 p(x) x dx \right],$$

which vanishes for small α . This means the algorithm slows down as the learning rate drops off, which is not surprising. However, the *conditional* probability of ending up at $x^1 = 1$ given that the

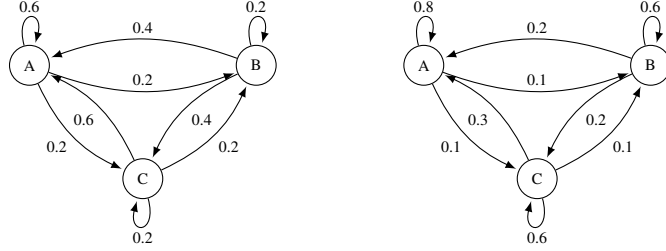


Figure 2: Markov chain example with 3 states. In the right figure, we halved each transition probability for moving between states, with the remaining probability put on the self-loop. Notice that halving all the transition probabilities would not change the equilibrium distribution, and instead would only increase the mixing time of the Markov chain.

algorithm did leave x^0 is

$$T_\alpha(0, 1 | x^1 \neq x^0) \approx \frac{T_\alpha(0, 1)}{T_\alpha(0, -1) + T_\alpha(0, 1)} = \frac{\int_0^\infty p(x)x \, dx}{\int_{-\infty}^0 p(x)x \, dx + \int_0^\infty p(x)x \, dx},$$

which does not depend on α . In other words, provided α is small, SR, on average, makes the same decisions/transitions with learning rate α as it does with learning rate $\alpha/10$; it just takes 10 times longer to make those decisions when $\alpha/10$ is used. In this situation, there is no exploitation benefit in dropping α .

The above argument is intuitive, but also informal. To make these statements rigorous, we interpret the SR method as a Markov chain. On each iteration, SR starts at some state (iterate) x , and moves to a new state y with some transition probability $T_\alpha(x, y)$ that depends only on x and the learning rate α . For fixed α , this is clearly a Markov process with transition matrix² $T_\alpha(x, y)$.

The long-term behavior of this Markov process is determined by the *stationary distribution* of $T_\alpha(x, y)$. We show below that for all small α , the stationary distribution of $T_\alpha(x, y)$ is nearly invariant to α , and thus decreasing α below some threshold has virtually no effect on the long term behavior of the method. This happens because, as α shrinks, the relative probabilities of leaving a state remain the same, even though the absolute probabilities decrease (see Figure 2). In this case, there is no exploitation benefit to decreasing α .

Theorem 5. *Let $p_{x,k}$ denote the probability distribution for the k th entry in $\nabla \tilde{f}(x)$, the stochastic gradient estimate at x . Assume there is a constant C_1 such that for all x , k , and ν we have $\int_\nu^\infty p_{x,k}(z) \, dz \leq \frac{C_1}{\nu^2}$, and some C_2 such that both $\int_0^{C_2} p_{x,k}(z) \, dz > 0$ and $\int_{-C_2}^0 p_{x,k}(z) \, dz > 0$. Define the matrix*

$$\tilde{U}(x, y) = \begin{cases} \int_0^\infty p_{x,k}(z) \frac{z}{\Delta} \, dz, & \text{if } x \text{ and } y \text{ differ only at coordinate } k, \text{ and } y_k = x_k + \Delta \\ \int_{-\infty}^0 p_{x,k}(z) \frac{z}{\Delta} \, dz, & \text{if } x \text{ and } y \text{ differ only at coordinate } k, \text{ and } y_k = x_k - \Delta \\ 0, & \text{otherwise,} \end{cases}$$

and the associated markov chain transition matrix

$$\tilde{T}_{\alpha_0} = I - \alpha_0 \cdot \text{diag}(\mathbf{1}^T \tilde{U}) + \alpha_0 \tilde{U}, \quad (8)$$

where α_0 is the largest constant that makes \tilde{T}_{α_0} non-negative. Suppose \tilde{T}_{α_0} has a stationary distribution, denoted $\tilde{\pi}$. Then, for sufficiently small α , T_α has a stationary distribution π_α , and

$$\lim_{\alpha \rightarrow 0} \pi_\alpha = \tilde{\pi}.$$

Furthermore, this limiting distribution satisfies $\tilde{\pi}(x) > 0$ for any state x , and is thus not concentrated on local minimizers of f .

²Our analysis below does not require the state space to be finite, so $T_\alpha(x, y)$ may be a linear operator rather than a matrix. Nonetheless, we use the term “matrix” as it is standard.

Table 1: Top-1 test or validation error after training with binarized initial weights.

	CIFAR-10				CIFAR-100	ImageNet
	VGG-9	VGG-BC	ResNet-56	WRN-56-2	ResNet-56	ResNet-18
ADAM	7.97	7.12	8.10	6.62	33.98	36.04
R-ADAM	23.99	21.88	33.56	27.90	68.39	91.07
BC-ADAM	10.36	8.21	8.83	7.17	35.34	52.11
SR-ADAM	23.33	20.56	26.49	21.58	58.06	88.86
Big SR-ADAM	16.95	16.77	19.84	16.04	50.79	77.68

While the long term stationary behavior of SR is relatively insensitive to α , the convergence speed of the algorithm is not. To measure this, we consider the *mixing time* of the Markov chain. Let π_α denote the stationary distribution of a Markov chain. We say that the ϵ -mixing time of the chain is M_ϵ if M_ϵ is the smallest integer such that [22]

$$|\mathbb{P}(x^{M_\epsilon} \in A | x^0) - \pi(A)| \leq \epsilon, \quad \text{for all } x^0 \text{ and all subsets of states } A \subseteq X. \quad (9)$$

We show below that the mixing time of the Markov chain gets large for small α , which means exploration slows down, even though no exploitation gain is being realized.

Theorem 6. *Let $p_{x,k}$ satisfy the assumptions of Theorem 5. Choose some ϵ sufficiently small that there exists a proper subset of states $A \subset X$ with stationary probability $\pi_\alpha(A)$ greater than ϵ . Let $M_\epsilon(\alpha)$ denote the ϵ -mixing time of the chain with learning rate α . Then,*

$$\lim_{\alpha \rightarrow 0} M_\epsilon(\alpha) = \infty.$$

6 Experiments

To explore the implications of the theory above, we train two types of networks, VGG-like CNNs [23] and Residual networks [24], on CIFAR-10/100 [25] and ImageNet 2012 [26]. VGG-9 on CIFAR-10 consists of 7 convolutional layers and 2 fully connected layers, with Batch Normalization [27] after each convolutional layer and the first linear layer (details of the VGG-9 architecture is in the Appendixes). VGG-BC is a high-capacity network used for the original BC model [3]. We use the same architecture as in [3] except using softmax and cross-entropy loss instead of SVM and squared hinge loss, respectively. ResNets-56 has 55 convolutional layers and one linear layer, and contains three stages of residual blocks where each stage has the same number of residual blocks. Similary, ResNets-18 for ImageNet has the same description as in [24]. We also create a wide ResNet-56 (WRN-56-2) that doubles the number of filters in each residual block as in [28]. We use ADAM [29] as the baseline optimizer, and train with the three quantized algorithms mentioned in Section 3, i.e., R-ADAM, SR-ADAM and BC-ADAM. All methods start with the same binary weight initialization of random ± 1 s. The image pre-processing and data augmentation procedures are the same as [24]. Similar to [4], here we only quantize the weights in the convolutional layers, but not linear layers, during training. We set the initial learning rate to 0.01 and decrease the learning rate by a factor of 10 at epochs 82 and 122 for CIFAR-10 and CIFAR-100 [24]. For ImageNet experiments, we train models for 90 epochs and decrease the learning rate at epoch 30 and 60. The default minibatch size is 128. The Big SR-ADAM method adopts a large minibatch size (512 for WRN-56-2 and ResNet-18 and 1024 for other models). Following [3], we do not use weight decay during training. We implement all quantization algorithms in Torch7 [30] and train the quantized models with NVIDIA GPUs.

Results The overall results are summarized in Table 1. The binary model trained by BC-ADAM has comparable performance to the full-precision model trained by ADAM. SR-ADAM outperforms R-ADAM, which verifies the effectiveness of Stochastic Rounding. There is a performance gap between SR-ADAM and BC-ADAM across all models and datasets. This is consistent with our theoretical results in Sections 4 and 5, and keeping track of the real-valued weights to quantize the binary weights in BC-ADAM seems to really help empirically.

Exploration vs exploitation tradeoffs Section 5 discusses the exploration/exploitation tradeoff of continuous-valued SGD methods and predicts that fully discrete methods like SR are unable to enter an exploitative phase. To test this effect, we plot the percentage of changed weights (signs different from the initialization) as a function of training epoch (Figure 3). SR-ADAM changes more weights

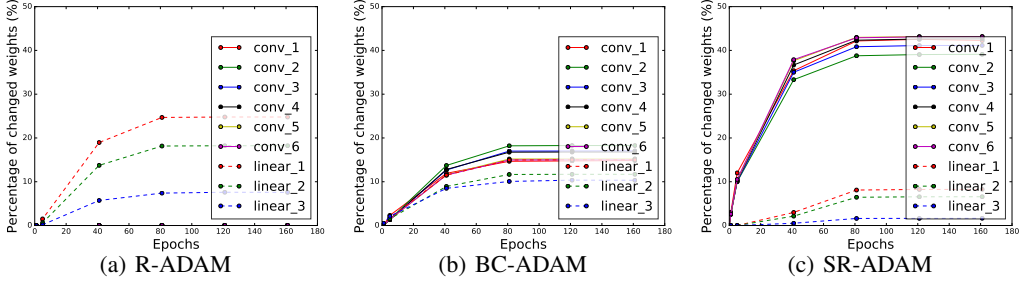


Figure 3: Percentage of weight changes during training of VGG-BC on CIFAR-10.

in the conv layers than both R-ADAM and BC-ADAM. The BC method never changes more than 20% of the weights (Fig 3(b)). This indicates that BC is able to change from explorative to exploitative - it drives more towards local minimizers and explores less aggressively. The SR method is never able to exit the exploration phase; it keeps changing weights until 50% of the weights differ from their starting values (in a binary model, randomly re-assigning weights would also result in 50% change). We see that the weights of the conv layers were not changed at all by R-ADAM. When the tails of the stochastic gradient distribution are light, this method is ineffective.

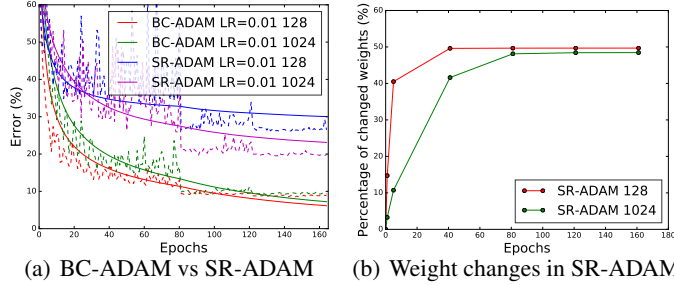


Figure 4: Effect of batch size on SR-ADAM when tested with ResNet-56 on CIFAR-10. (a) Test error vs epoch. Test error is reported with dashed lines, train error with solid lines. Results reported for batch size 128 and 1024.

Effect of Batch Size We saw from Figure 1, that SR is unable to become exploitative because, for small learning rates α , we are only decreasing the likelihood of moving, and not creating any bias towards moving downhill vs. uphill. To verify that this is a source of the problems that we observe with SR, we increase the batch size. By doing this, we shrink the variance of the gradient distribution in Figure 1 without changing the mean. This weights the gradient proposal distribution towards downhill directions, making the algorithm more exploitative. Our theory predicts that this should help mitigate the problem of SR being unable to exploit local minima by decreasing the learning rate. Figure 4(a) illustrates the effect of large batch size for BC and SR methods. We find that a small batch size yields better performance for BC methods while a large batch size is essential for the SR method. Figure 4(b) shows the percentage of weights changed by SR since initialization for ResNet-56. With batch size 128, 40% weights have changed by epoch 5 while only 10% weights changed with batch size 1024. This shows that exploration has slowed down; the algorithm has more of an affinity for its local neighborhood. As predicted, this enables SR to decrease the objective, and both training and test error drops by roughly 8% (Figure 4(a)). Table 1 shows that increasing the batch size (Big SR-ADAM) leads to improved performance over SR-ADAM consistently.

7 Conclusion

The training of quantized neural networks is essential for deploying machine learning models on embedded and ubiquitous devices. In this work, we provided a theoretical analysis to better understand the BinaryConnect (BC) and Stochastic Rounding (SR) methods for training binary neural networks. We proved convergence results for BC and SR methods that provide convergence rates and predict an accuracy bound that depends on the coarseness of discretization. For general non-convex problems, we proved that SR differs from conventional stochastic methods in that it is unable to exploit greedy local search. Experiments confirm these findings, and show that the mathematical properties of SR are indeed observable (and very important) in practice.

References

- [1] Courbariaux, M., Hubara, I., Soudry, D., El-Yaniv, R., Bengio, Y.: Binarized neural networks: Training deep neural networks with weights and activations constrained to +1 or -1. arXiv preprint arXiv:1602.02830 (2016)
- [2] Marchesi, M., Orlandi, G., Piazza, F., Uncini, A.: Fast neural networks without multipliers. *IEEE Transactions on Neural Networks* **4**(1) (1993) 53–62
- [3] Courbariaux, M., Bengio, Y., David, J.P.: Binaryconnect: Training deep neural networks with binary weights during propagations. In: NIPS. (2015)
- [4] Rastegari, M., Ordonez, V., Redmon, J., Farhadi, A.: XNOR-Net: ImageNet Classification Using Binary Convolutional Neural Networks. ECCV (2016)
- [5] Gupta, S., Agrawal, A., Gopalakrishnan, K., Narayanan, P.: Deep learning with limited numerical precision. In: ICML. (2015)
- [6] Lin, D., Talathi, S., Annapureddy, S.: Fixed point quantization of deep convolutional networks. In: ICML. (2016)
- [7] Hwang, K., Sung, W.: Fixed-point feedforward deep neural network design using weights+ 1, 0, and- 1. In: IEEE Workshop on Signal Processing Systems (SiPS). (2014)
- [8] Lin, Z., Courbariaux, M., Memisevic, R., Bengio, Y.: Neural networks with few multiplications. ICLR (2016)
- [9] Li, F., Zhang, B., Liu, B.: Ternary weight networks. arXiv preprint arXiv:1605.04711 (2016)
- [10] Kim, M., Smaragdis, P.: Bitwise neural networks. In: ICML Workshop on Resource-Efficient Machine Learning. (2015)
- [11] Hubara, I., Courbariaux, M., Soudry, D., El-Yaniv, R., Bengio, Y.: Quantized neural networks: Training neural networks with low precision weights and activations. arXiv preprint arXiv:1609.07061 (2016)
- [12] Baldassi, C., Ingrosso, A., Lucibello, C., Saglietti, L., Zecchina, R.: Subdominant dense clusters allow for simple learning and high computational performance in neural networks with discrete synapses. *Physical review letters* **115**(12) (2015) 128101
- [13] Anwar, S., Hwang, K., Sung, W.: Fixed point optimization of deep convolutional neural networks for object recognition. In: ICASSP, IEEE (2015)
- [14] Zhu, C., Han, S., Mao, H., Dally, W.J.: Trained ternary quantization. ICLR (2017)
- [15] Zhou, A., Yao, A., Guo, Y., Xu, L., Chen, Y.: Incremental network quantization: Towards lossless cnns with low-precision weights. ICLR (2017)
- [16] Zhou, S., Wu, Y., Ni, Z., Zhou, X., Wen, H., Zou, Y.: Dorefa-net: Training low bitwidth convolutional neural networks with low bitwidth gradients. arXiv preprint arXiv:1606.06160 (2016)
- [17] Höhfeld, M., Fahlman, S.E.: Probabilistic rounding in neural network learning with limited precision. *Neurocomputing* **4**(6) (1992) 291–299
- [18] Miyashita, D., Lee, E.H., Murmann, B.: Convolutional neural networks using logarithmic data representation. arXiv preprint arXiv:1603.01025 (2016)
- [19] Soudry, D., Hubara, I., Meir, R.: Expectation backpropagation: Parameter-free training of multilayer neural networks with continuous or discrete weights. In: NIPS. (2014)
- [20] Cheng, Z., Soudry, D., Mao, Z., Lan, Z.: Training binary multilayer neural networks for image classification using expectation backpropagation. arXiv preprint arXiv:1503.03562 (2015)
- [21] Lan, G., Nemirovski, A., Shapiro, A.: Validation analysis of mirror descent stochastic approximation method. *Mathematical programming* **134**(2) (2012) 425–458
- [22] Levin, D.A., Peres, Y., Wilmer, E.L.: Markov chains and mixing times. American Mathematical Soc. (2009)
- [23] Simonyan, K., Zisserman, A.: Very Deep Convolutional Networks for Large-Scale Image Recognition. In: ICLR. (2015)

- [24] He, K., Zhang, X., Ren, S., Sun, J.: Deep Residual Learning for Image Recognition. In: CVPR. (2016)
- [25] Krizhevsky, A.: Learning multiple layers of features from tiny images. (2009)
- [26] Russakovsky, O., Deng, J., Su, H., Krause, J., Satheesh, S., Ma, S., Huang, Z., Karpathy, A., Khosla, A., Bernstein, M., et al.: Imagenet Large Scale Visual Recognition Challenge. IJCV (2015)
- [27] Ioffe, S., Szegedy, C.: Batch normalization: Accelerating deep network training by reducing internal covariate shift. ICML (2015)
- [28] Zagoruyko, S., Komodakis, N.: Wide residual networks. arXiv preprint arXiv:1605.07146 (2016)
- [29] Kingma, D., Ba, J.: Adam: A method for stochastic optimization. ICLR (2015)
- [30] Collobert, R., Kavukcuoglu, K., Farabet, C.: Torch7: A matlab-like environment for machine learning. In: BigLearn, NIPS Workshop. (2011)
- [31] Lax, P.: Linear Algebra and Its Applications. Number v. 10 in Linear algebra and its applications. Wiley (2007)

Training Quantized Nets: A Deeper Understanding

Appendices

Here we present proofs of the lemmas and theorems presented in the main paper, as well as some additional experimental details and results.

A Proof of Lemma 1

Proof. We want to bound the quantization error r^t . Consider the i -th entry in r^t denoted by r_i^t . Similarly, we define w_i^t and $\nabla \tilde{f}(w^t)_i$. Choose some random number $p \in [0, 1]$. The stochastic rounding operation produces a value of r^t given by

$$\begin{aligned} r_i^t &= Q_s(w_i^t - \alpha_t \nabla \tilde{f}(w^t)_i) - w_i^t + \alpha_t \nabla \tilde{f}(w^t)_i \\ &= \Delta \cdot \begin{cases} \frac{\alpha_t \nabla \tilde{f}(w^t)_i}{\Delta} + \left\lfloor \frac{-\alpha_t \nabla \tilde{f}(w^t)_i}{\Delta} \right\rfloor + 1, & \text{for } p \leq q, \\ \frac{\alpha_t \nabla \tilde{f}(w^t)_i}{\Delta} + \left\lfloor \frac{-\alpha_t \nabla \tilde{f}(w^t)_i}{\Delta} \right\rfloor, & \text{otherwise.} \end{cases} \\ &= \Delta \cdot \begin{cases} -q + 1, & \text{for } p \leq q, \\ -q, & \text{otherwise.} \end{cases} \end{aligned}$$

where we write $q = -\frac{\alpha_t \nabla \tilde{f}(w^t)_i}{\Delta} - \left\lfloor \frac{-\alpha_t \nabla \tilde{f}(w^t)_i}{\Delta} \right\rfloor$ and $q \in [0, 1]$.

Now we have

$$\begin{aligned} \mathbb{E}_p[(r_i^t)^2] &\leq \Delta^2((-q+1)^2q + (-q)^2(1-q)) \\ &= \Delta^2q(1-q) \\ &\leq \Delta^2 \min\{q, 1-q\}. \end{aligned}$$

Because $\min\{q, 1-q\} \leq \left| \frac{\alpha_t \nabla \tilde{f}(w^t)_i}{\Delta} \right|$, it follows that $\mathbb{E}_p[(r_i^t)^2] \leq \Delta^2 \left| \frac{\alpha_t \nabla \tilde{f}(w^t)_i}{\Delta} \right| \leq \Delta \left| \alpha_t \nabla \tilde{f}(w^t)_i \right|$.

Summing over the index i yields

$$\begin{aligned} \mathbb{E}_p \|r^t\|_2^2 &\leq \Delta \alpha_t \|\nabla \tilde{f}(w^t)\|_1 \\ &\leq \sqrt{d} \alpha_t \Delta \|\nabla \tilde{f}(w^t)\|_2. \end{aligned} \tag{10}$$

Now, $(\mathbb{E} \|\nabla \tilde{f}(w^t)\|_2)^2 \leq \mathbb{E} \|\nabla \tilde{f}(w^t)\|_2^2 \leq G^2$. Plugging this into (10) yields

$$\mathbb{E} \|r^t\|_2^2 \leq \sqrt{d} \Delta \alpha_t G. \tag{11}$$

□

B Proof of Theorem 1

Proof. From the update rule (6), we get:

$$\begin{aligned} w^{t+1} &= Q(w^t - \alpha_t \nabla \tilde{f}(w^t)) \\ &= w^t - \alpha_t \nabla \tilde{f}(w^t) + r^t, \end{aligned}$$

where r^t denotes the quantization used on the t -th iteration. Subtracting by the optimal w^* , taking norm, and taking expectation conditioned on w^t , we get:

$$\begin{aligned} \mathbb{E} \|w^{t+1} - w^*\|^2 &= \|w^t - w^*\|^2 - 2\mathbb{E} \langle w^t - w^*, \alpha_t \nabla \tilde{f}(w^t) - r^t \rangle + \mathbb{E} \|\alpha_t \nabla \tilde{f}(w^t) - r^t\|^2 \\ &= \|w^t - w^*\|^2 - 2\alpha_t \langle w^t - w^*, \nabla F(w^t) \rangle + \alpha_t^2 \mathbb{E} \|\nabla \tilde{f}(w^t)\|^2 + \mathbb{E} \|r^t\|^2 \\ &\leq \|w^t - w^*\|^2 - 2\alpha_t \langle w^t - w^*, \nabla F(w^t) \rangle + \alpha_t^2 G^2 + \sqrt{d} \Delta \alpha_t G, \end{aligned}$$

where we use the bounded variance assumption, $\mathbb{E}[r^t] = 0$, and Lemma 1. Using the assumption that F is μ -strongly convex, we can simplify this to:

$$\mathbb{E} \|w^{t+1} - w^*\|^2 \leq (1 - \alpha_t \mu) \|w^t - w^*\|^2 - 2\alpha_t (F(w^t) - F(w^*)) + \alpha_t^2 G^2 + \sqrt{d} \Delta \alpha_t G.$$

Re-arranging the terms, and taking expectation we get:

$$\begin{aligned} 2\alpha_t \mathbb{E}(F(w^t) - F(w^*)) &\leq (1 - \alpha_t \mu) \mathbb{E}\|w^t - w^*\|^2 - \mathbb{E}\|w^{t+1} - w^*\|^2 + \alpha_t^2 G^2 + \sqrt{d} \Delta \alpha_t G. \\ \Rightarrow \mathbb{E}(F(w^t) - F(w^*)) &\leq \left(\frac{1}{2\alpha_t} - \frac{\mu}{2} \right) \mathbb{E}\|w^t - w^*\|^2 - \frac{1}{2\alpha_t} \mathbb{E}\|w^{t+1} - w^*\|^2 + \frac{\alpha_t}{2} G^2 + \frac{\sqrt{d} \Delta G}{2}. \end{aligned}$$

Assume that the stepsize decreases with the rate $\alpha_t = 1/\mu(t+1)$. Then we have:

$$\mathbb{E}(F(w^t) - F(w^*)) \leq \frac{\mu t}{2} \mathbb{E}\|w^t - w^*\|^2 - \frac{\mu(t+1)}{2} \mathbb{E}\|w^{t+1} - w^*\|^2 + \frac{1}{2\mu(t+1)} G^2 + \frac{\sqrt{d} \Delta G}{2}.$$

Averaging over $t = 0$ to T , we get a telescoping sum on the right hand side, which yields:

$$\begin{aligned} \frac{1}{T} \sum_{t=0}^T \mathbb{E}(F(w^t) - F(w^*)) &\leq \frac{G^2}{2\mu T} \sum_{t=0}^T \frac{1}{t+1} + \frac{\sqrt{d} \Delta G}{2} - \frac{\mu(T+1)}{2} \mathbb{E}\|w^{T+1} - w^*\|^2 \\ &\leq \frac{(1 + \log(T+1))G^2}{2\mu T} + \frac{\sqrt{d} \Delta G}{2}. \end{aligned}$$

Using Jensen's inequality, we have:

$$\mathbb{E}(F(\bar{w}^T) - F(w^*)) \leq \frac{1}{T} \sum_{t=0}^T \mathbb{E}(F(w^t) - F(w^*)),$$

where $\bar{w}^T = \frac{1}{T} \sum_{t=0}^T w^t$, the average of the iterates.

Thus the final convergence theorem is given by:

$$\mathbb{E}[F(\bar{w}^T) - F(w^*)] \leq \frac{(1 + \log(T+1))G^2}{2\mu T} + \frac{\sqrt{d} \Delta G}{2}.$$

□

C Proof of Theorem 2

Proof. From the update rule (6), we have,

$$w^{t+1} = Q(w^t - \alpha_t \nabla \tilde{f}(w^t)) = w^t - \alpha_t \nabla \tilde{f}(w^t) + r^t,$$

where r^t denotes the quantization error on the t -th iteration. Hence we have

$$\begin{aligned} \|w^{t+1} - w^*\|^2 &= \|w^t - \alpha_t \nabla \tilde{f}(w^t) + r^t - w^*\|^2 \\ &= \|w^t - w^*\|^2 - 2\langle w^t - w^*, \alpha_t \nabla \tilde{f}(w^t) - r^t \rangle + \|\alpha_t \nabla \tilde{f}(w^t) - r^t\|^2. \end{aligned}$$

Taking expectation, and using $\mathbb{E}[\tilde{f}(w^t)] = \nabla F(w^t)$ and $\mathbb{E}[r^t] = 0$, we have

$$\begin{aligned} \mathbb{E}\|w^{t+1} - w^*\|^2 &= \mathbb{E}\|w^t - w^*\|^2 - 2\alpha_t \mathbb{E}\langle w^t - w^*, \nabla F(w^t) \rangle + \mathbb{E}\|\alpha_t \nabla \tilde{f}(w^t) - r^t\|^2 \\ &= \mathbb{E}\|w^t - w^*\|^2 - 2\alpha_t \mathbb{E}\langle w^t - w^*, \nabla F(w^t) \rangle + \alpha_t^2 \mathbb{E}\|\nabla \tilde{f}(w^t)\|^2 + \mathbb{E}\|r^t\|^2. \end{aligned}$$

Using the bounded variance assumption $\mathbb{E}\|\nabla \tilde{f}(w^t)\|^2 \leq G^2$ and bounded quantization error in Lemma 1, we have

$$\mathbb{E}\|w^{t+1} - w^*\|^2 \leq \mathbb{E}\|w^t - w^*\|^2 - 2\alpha_t \mathbb{E}\langle w^t - w^*, \nabla F(w^t) \rangle + \alpha_t^2 G^2 + \sqrt{d} \Delta \alpha_t G. \quad (12)$$

$F(x)$ is convex and hence $\langle \nabla F(x), x_t - x^* \rangle \geq F(x_t) - F(x^*)$, which can be used in (12) to get

$$\mathbb{E}\|w^{t+1} - w^*\|^2 \leq \mathbb{E}\|w^t - w^*\|^2 - 2\alpha_t \mathbb{E}[F(w^t) - F(w^*)] + \alpha_t^2 G^2 + \sqrt{d} \Delta \alpha_t G.$$

Re-arranging the terms, we have,

$$\mathbb{E}[F(w^t) - F(w^*)] \leq \frac{1}{2\alpha_t} (\mathbb{E}\|w^t - w^*\|^2 - \mathbb{E}\|w^{t+1} - w^*\|^2) + \frac{\alpha_t}{2} G^2 + \frac{1}{2} \sqrt{d} \Delta G.$$

Accumulate from $t = 1$ to T , we have

$$\begin{aligned} \sum_{t=1}^T \mathbb{E}[F(w^t) - F(w^*)] &\leq \frac{1}{2\alpha_1} \mathbb{E}\|w_1 - w^*\|^2 + \sum_{t=1}^T \left(\frac{1}{2\alpha_t} - \frac{1}{2\alpha_{t-1}} \right) \mathbb{E}\|w^t - w^*\|^2 \\ &\quad + \sum_{t=1}^T \frac{\alpha_t}{2} G^2 + \frac{T}{2} \sqrt{d} \Delta G. \end{aligned}$$

Applying $\mathbb{E}\|w^t - w^*\|^2 \leq D^2$ and $\sum_{t=1}^T \alpha_t \leq c\sqrt{T+1}$, we have

$$\sum_{t=1}^T \mathbb{E}[F(w^t) - F(w^*)] \leq \frac{\sqrt{T}}{2c} D^2 + \frac{c\sqrt{T+1}}{2} G^2 + \frac{T}{2} \sqrt{d} \Delta G. \quad (13)$$

Since $F(w)$ is convex, for $\bar{w}^T = \frac{1}{T} \sum_{t=1}^T w^t$, we have

$$\mathbb{E}[F(\bar{w}^T) - F(w^*)] \leq \frac{1}{T} \sum_{t=1}^T \mathbb{E}[F(w^t) - F(w^*)]. \quad (14)$$

Combine (13) and (14) to achieve

$$\mathbb{E}[F(\bar{w}^T) - F(w^*)] \leq \frac{1}{2c\sqrt{T}} D^2 + \frac{\sqrt{T+1}}{2T} c G^2 + \frac{\sqrt{d}\Delta G}{2}.$$

□

D Proof of Theorem 3

Proof. From the update rule (7), we have,

$$w^{t+1} = w^t - \alpha_t \nabla \tilde{f}(Q(w^t)) = w^t - \alpha_t \nabla \tilde{f}(w^t + r^t).$$

Taking expectation conditioned on w^t and r^t , we have

$$\begin{aligned} & \mathbb{E}\|w^{t+1} - w^*\|^2 \\ &= \mathbb{E}\|w^t - \alpha_t \nabla \tilde{f}(w^t + r^t) - w^*\|^2 \\ &= \mathbb{E}\|w^t - \alpha_t \nabla \tilde{f}(w^t) + \alpha_t \nabla \tilde{f}(w^t) - \alpha_t \nabla \tilde{f}(w^t + r^t) - w^*\|^2 \\ &= \|w^t - w^*\|^2 - 2\alpha_t \mathbb{E}\langle w^t - w^*, \nabla \tilde{f}(w^t) \rangle + 2\alpha_t \mathbb{E}\langle w^t - w^*, \nabla \tilde{f}(w^t) - \nabla \tilde{f}(w^t + r^t) \rangle + \mathbb{E}\|\alpha_t \nabla \tilde{f}(w^t + r^t)\|^2 \\ &= \|w^t - w^*\|^2 - 2\alpha_t \langle w^t - w^*, \nabla F(w^t) \rangle + 2\alpha_t \langle w^t - w^*, \nabla F(w^t) - \nabla F(w^t + r^t) \rangle + \alpha_t^2 \mathbb{E}\|\nabla \tilde{f}(w^t + r^t)\|^2 \\ &\leq \|w^t - w^*\|^2 - 2\alpha_t \langle w^t - w^*, \nabla F(w^t) \rangle + 2\alpha_t \|w^t - w^*\| \|\nabla F(w^t) - \nabla F(w^t + r^t)\| + \alpha_t^2 G^2 \\ &\leq \|w^t - w^*\|^2 - 2\alpha_t \langle w^t - w^*, \nabla F(w^t) \rangle + 2\alpha_t L \|r^t\| \|w^t - w^*\| + \alpha_t^2 G^2. \end{aligned}$$

Using $\|r^t\| \leq \sqrt{d}\Delta$ and bounded domain assumption, we get

$$\begin{aligned} \mathbb{E}\|w^{t+1} - w^*\|^2 &\leq \|w^t - w^*\|^2 - 2\alpha_t \langle w^t - w^*, \nabla F(w^t) \rangle + 2\alpha_t L \sqrt{d}\Delta \|w^t - w^*\| + \alpha_t^2 G^2 \\ &\leq \|w^t - w^*\|^2 - 2\alpha_t \langle w^t - w^*, \nabla F(w^t) \rangle + 2\alpha_t L \sqrt{d}\Delta D + \alpha_t^2 G^2. \end{aligned}$$

Taking expectation, and following the same steps as in Theorem 2, we get the convergence result:

$$\mathbb{E}[F(\bar{w}^T) - F(w^*)] \leq \frac{1}{2c\sqrt{T}} D^2 + \frac{\sqrt{T+1}}{2T} c G^2 + \sqrt{d}\Delta LD.$$

□

E Proof of Theorem 4

Proof. From the update rule (7), we get

$$\begin{aligned} w^{t+1} &= w^t - \alpha_t \nabla \tilde{f}(Q(w^t)) \\ &= w^t - \alpha_t \nabla \tilde{f}(w^t + r^t) \\ &= w^t - \alpha_t [\nabla \tilde{f}(w^t) + \nabla^2 \tilde{f}(w^t) r^t + \hat{r}^t] \end{aligned}$$

where $\|\hat{r}^t\| \leq \frac{L_2}{2} \|r^t\|^2$, from our assumption on the Hessian. Note that in general r^t has mean zero while \hat{r}^t does not. Using the same steps as in the Theorem 1, we get

$$\begin{aligned} \mathbb{E}\|w^{t+1} - w^*\|^2 &= \|w^t - w^*\|^2 - 2\alpha_t \mathbb{E}\langle w^t - w^*, \nabla \tilde{f}(w^t + r^t) \rangle + \alpha_t^2 \mathbb{E}\|\nabla \tilde{f}(w^t + r^t)\|^2 \\ &\leq \|w^t - w^*\|^2 - 2\alpha_t \mathbb{E}\langle w^t - w^*, \nabla F(w^t) + \hat{r}^t \rangle + \alpha_t^2 G^2 \\ &= \|w^t - w^*\|^2 - 2\alpha_t \mathbb{E}\langle w^t - w^*, \nabla F(w^t) \rangle + \alpha_t^2 G^2 - 2\alpha_t \mathbb{E}\langle w^t - w^*, \hat{r}^t \rangle \end{aligned}$$

Assuming the domain has finite diameter D , and observing that the quantization error for BC-SGD can always be upper-bounded as $\|r^t\| \leq \sqrt{d}\Delta$, we get:

$$-2\alpha_t \mathbb{E}\langle w^t - w^*, \hat{r}^t \rangle \leq 2\alpha_t D \mathbb{E}\|\hat{r}^t\| \leq 2\alpha_t D \frac{L_2}{2} \|r^t\| \leq \alpha_t D L_2 \sqrt{d}\Delta.$$

Following the same steps as in Theorem 1, we get

$$\mathbb{E}[F(\bar{w}^T) - F(w^*)] \leq \frac{(1 + \log(T + 1))G^2}{2\mu T} + \frac{DL_2\sqrt{d}\Delta}{2}.$$

□

F Proof of Theorem 5

Proof. Let the matrix U_α be a partial transition matrix defined by $U_\alpha(x, x) = 0$, and $U_\alpha(x, y) = T_\alpha(x, y)$ for $x \neq y$. From U_α , we can get back the full transition matrix T_α using the formula

$$T_\alpha = I - \text{diag}(\mathbf{1}^T U_\alpha) + U_\alpha.$$

Note that this formula is essentially “filling in” the diagonal entries of T_α so that every column sums to 1, thus making T_α a valid stochastic matrix.

Let’s bound the entries in U_α . Suppose that we begin an iteration of the stochastic rounding algorithm at some point x . Consider an adjacent point y that differs from x at only 1 coordinate, k , with $y_k = x_k + \Delta$. Then we have

$$\begin{aligned} U_\alpha(x, y) &= \frac{1}{\alpha} \int_0^\Delta p_{x,k}(x/\alpha) \frac{x}{\Delta} dx + \frac{1}{\alpha} \int_\Delta^{2\Delta} p_{x,k}(x/\alpha) \frac{2\Delta - x}{\Delta} dx \\ &= \frac{1}{\alpha} \int_0^{\Delta/\alpha} p_{x,k}(z) \frac{\alpha z}{\Delta} \alpha dz + \frac{1}{\alpha} \int_{\Delta/\alpha}^{2\Delta/\alpha} p_{x,k}(z) \frac{2\Delta - \alpha z}{\Delta} \alpha dz \\ &\leq \alpha \int_0^{\Delta/\alpha} p_{x,k}(z) \frac{z}{\Delta} dz + \int_{\Delta/\alpha}^\infty p_{x,k}(z) dz \\ &= \alpha \int_0^\infty p_{x,k}(z) \frac{z}{\Delta} dz + O(\alpha^2). \end{aligned} \tag{15}$$

Note we have used the decay assumption:

$$\int_\nu^\infty p_{x,k}(z) dz \leq \frac{C}{\nu^2}.$$

Likewise, if $y_k = x_k - \Delta$, then the transition probability is

$$U_\alpha(x, y) = \alpha \int_{-\infty}^0 p_{x,k}(z) \frac{z}{\Delta} dz + O(\alpha^2), \tag{16}$$

and if $y_k = x_k \pm m\Delta$ for an integer $m > 1$,

$$U_\alpha(x, y) = O(\alpha^2). \tag{17}$$

We can approximate the behavior of U_α using the matrix $\tilde{U}(x, y)$, and we define the associated markov chain transition matrix \tilde{T}_α as in (8).

Let α_0 be the largest scalar such that the stochastic linear operator \tilde{T}_{α_0} has non-negative entries. For $\alpha < \alpha_0$, \tilde{T}_α has non-negative entries and column sums equal to 1; it thus defines the transition operator of a markov chain. Let $\tilde{\pi}$ denote the stationary distribution of the markov chain with transition matrix \tilde{T}_{α_0} .

We now claim that $\tilde{\pi}$ is also the stationary distribution of \tilde{T}_α for all $\alpha < \alpha_0$. We verify this by noting that

$$\begin{aligned} \tilde{T}_\alpha &= (I - \alpha \cdot \text{diag}(\mathbf{1}^T \tilde{U}))\tilde{\pi} + \alpha \tilde{U} \tilde{\pi} \\ &= (1 - \frac{\alpha}{\alpha_0})I + \frac{\alpha}{\alpha_0} [I - \alpha_0 \cdot \text{diag}(\mathbf{1}^T \tilde{U}) + \alpha_0 \tilde{U}] \\ &= (1 - \frac{\alpha}{\alpha_0})I + \frac{\alpha}{\alpha_0} \tilde{T}_{\alpha_0} \end{aligned} \tag{18}$$

and so $\tilde{T}_\alpha \tilde{\pi} = (1 - \frac{\alpha}{\alpha_0})\tilde{\pi} + \frac{\alpha}{\alpha_0} \tilde{\pi} = \tilde{\pi}$.

Recall that T_α is the transition matrix for the Markov chain generated by the stochastic rounding algorithm with learning rate α . We wish to show that this markov chain is well approximated by \tilde{T}_α . Note that

$$T_\alpha(x, y) = \prod_{k, x_k \neq y_k} T_\alpha(x, x + (y_k - x_k)\Delta e_k) \leq O(\alpha^2)$$

when x, y differ at more than 1 coordinate. In other words, transitions between multiple coordinates simultaneously become vanishingly unlikely for small α . When x and y differ by exactly 1 coordinate, we know from (15) that

$$T_\alpha(x, y) = \alpha U(x, y) + O(\alpha^2).$$

These observations show that the off-diagonal elements of T_α are well approximated (up to uniform $O(\alpha^2)$ error) by the corresponding elements in αU . Since the columns of T_α sum to one, the diagonal elements are well approximated as well, and we have

$$T_\alpha = (I - \alpha \cdot \text{diag}(\mathbf{1}^T U)) + \alpha U + O(\alpha^2) = \tilde{T}_\alpha + O(\alpha^2).$$

To be precise, the notation above means that

$$|T_\alpha(x, y) - \tilde{T}_\alpha(x, y)| < C\alpha^2, \quad (19)$$

for some C that is uniform over (x, y) .

We are now ready to show that the stationary distribution of T_α exists and approaches $\tilde{\pi}$. Re-arranging (18) gives us

$$\alpha_0 \tilde{T}_\alpha + (\alpha - \alpha_0)I = \alpha \tilde{T}_{\alpha_0}.$$

Combining this with (19), we get

$$\|\alpha_0 T_\alpha + (\alpha - \alpha_0)I - \alpha \tilde{T}_{\alpha_0}\|_\infty < O(\alpha^2),$$

and so

$$\|\frac{\alpha_0}{\alpha} T_\alpha + (1 - \frac{\alpha_0}{\alpha})I - \tilde{T}_{\alpha_0}\|_\infty < O(\alpha). \quad (20)$$

From (20), we see that the matrix $\frac{\alpha_0}{\alpha} T_\alpha + (1 - \frac{\alpha_0}{\alpha})I$ approaches \tilde{T}_{α_0} . Note that $\tilde{\pi}$ is the Perron-Frobenius eigenvalue of \tilde{T}_{α_0} , and thus has multiplicity 1. Multiplicity 1 eigenvalues/vectors of a matrix vary continuously with small perturbations to that matrix (Theorem 8, p130 of [31]). It follows that, for small α , $\frac{\alpha_0}{\alpha} T_\alpha + (1 - \frac{\alpha_0}{\alpha})I$ has a stationary distribution, and this distribution approaches $\tilde{\pi}$. The leading eigenvector of $\frac{\alpha_0}{\alpha} T_\alpha + (1 - \frac{\alpha_0}{\alpha})I$ is the same as the leading eigenvector of T_α , and it follows that T_α has a stationary distribution that approaches $\tilde{\pi}$.

Finally, note that we have assumed $\int_0^{C_2} p_{x,k}(z) dz > 0$ and $\int_{-C_2}^0 p_{x,k}(z) dz > 0$. Under this assumption, for $\alpha < \frac{1}{C_2}$, $\tilde{T}_{\alpha_0}(x, y) > 0$ whenever x, y are neighbors the differ at a single coordinate. It follows that every state in the Markov chain \tilde{T}_{α_0} is accessible from every other state by traversing a path of non-zero transition probabilities, and so $\tilde{\pi}(x) > 0$ for every state x . \square

G Proof of Theorem 6

Proof. Given some distribution π over the states of the markov chain, and some set A of states, let $[\pi]_A = \sum_{a \in A} \pi(a)$ denote the measure of A with respect to π .

Suppose for contradiction that the mixing time of the chain remains bounded as α vanishes. Then we can find an integer M_ϵ that upper bounds the ϵ -mixing time for all α . By the assumption of the theorem, we can select some set of states A with $[\tilde{\pi}]_A > \epsilon$, and some starting state $y \notin A$. Let e be a distribution (a vector in the finite-state case) with $e_y = 1$, $e_k = 0$ for $k \neq y$. Note that $[e]_A = 0$ because $y \notin A$. Then

$$|[e]_A - [\tilde{\pi}]_A| > \epsilon.$$

Note that, as $\alpha \rightarrow 0$, we have $\|T_\alpha - \tilde{T}_\alpha\| \rightarrow 0$ and thus $\|T_\alpha^{M_\epsilon} - \tilde{T}_\alpha^{M_\epsilon}\| \rightarrow 0$. We also see from the definition of \tilde{T}_α in (8), $\lim_{\alpha \rightarrow 0} \tilde{T}_\alpha = I$. It follows that

$$\lim_{\alpha \rightarrow 0} |[T_\alpha^{M_\epsilon} e]_A - [\tilde{\pi}]_A| = |[e]_A - [\tilde{\pi}]_A| > \epsilon,$$

and so for some α the inequality (9) is violated. This is a contradiction because it was assumed M_ϵ is an upper bound on the mixing time. \square

Table 2: VGG-9 on CIFAR-10.

layer type	input size	output size
Conv_1	$3 \times 32 \times 32$	$64 \times 32 \times 32$
Conv_2	$64 \times 32 \times 32$	$64 \times 32 \times 32$
MP	$64 \times 32 \times 32$	$64 \times 16 \times 16$
Conv_3	$64 \times 16 \times 16$	$128 \times 16 \times 16$
Conv_4	$128 \times 16 \times 16$	$128 \times 16 \times 16$
MP	$128 \times 16 \times 16$	$128 \times 8 \times 8$
Conv_5	$128 \times 8 \times 8$	$256 \times 8 \times 8$
Conv_6	$256 \times 8 \times 8$	$256 \times 8 \times 8$
Conv_7	$256 \times 8 \times 8$	$256 \times 8 \times 8$
MP	$256 \times 8 \times 8$	$256 \times 4 \times 4$
Linear	1×4096	1×256
Linear	1×256	1×10

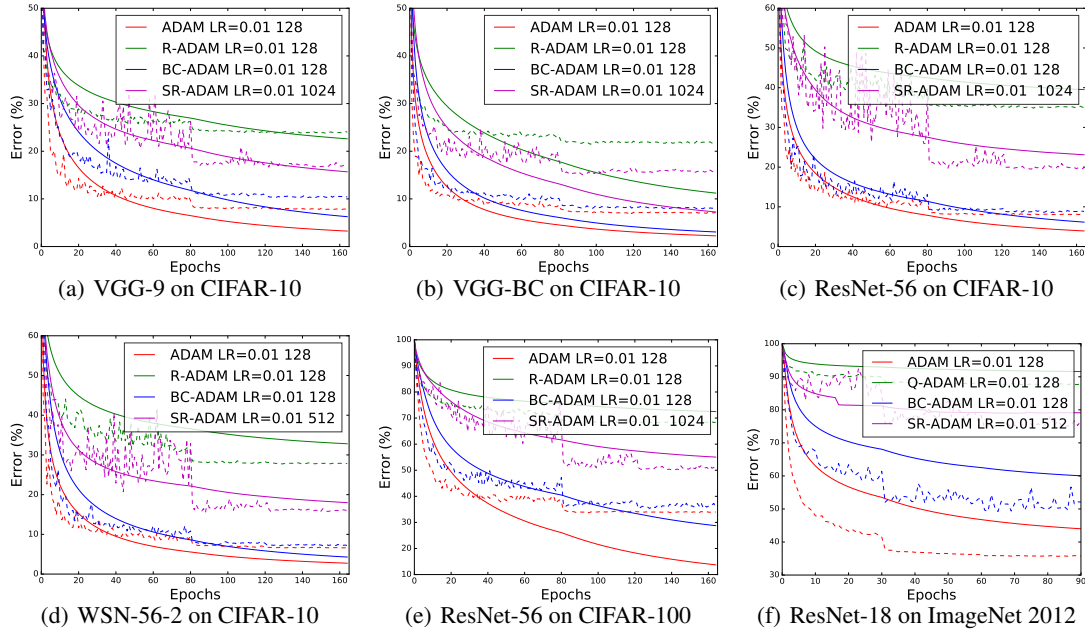


Figure 5: Training and testing errors of different training methods for VGG-9, VGG-BC, ResNet-56, Wide-ResNet-56-2 and ResNet-18. The solid line is the training error and the dashed line is the testing error.

H Additional Experimental Details & Results

H.1 VGG-9 Architecture

VGG-9 on CIFAR-10 consists of 7 convolutional layers and 2 fully connected (linear) layers. The convolutional layers contain 64, 64, 128, 128, 256, 256 and 256 of 3×3 filters respectively. There is a Batch Normalization and ReLU after each convolutional layer and the first fully connected layer. The details of the architecture is presented in Table 2.

H.2 Convergence Curves

The convergence curves for training and testing errors reported in Table 1 are shown in Figure 5.

H.3 Weight Initialization and Learning Rate

The authors of BC [3] adopt a small initial learning rate (0.003) and it takes 500 epochs to converge. It is observed that large binary weights ($s = 1$) will generate small gradients, hence a large learning rate is necessary for faster convergence. We experiment with a larger learning rate (0.01) and find it converges to the same performance within 160 epochs, comparing with 500 epochs in the original paper [3].

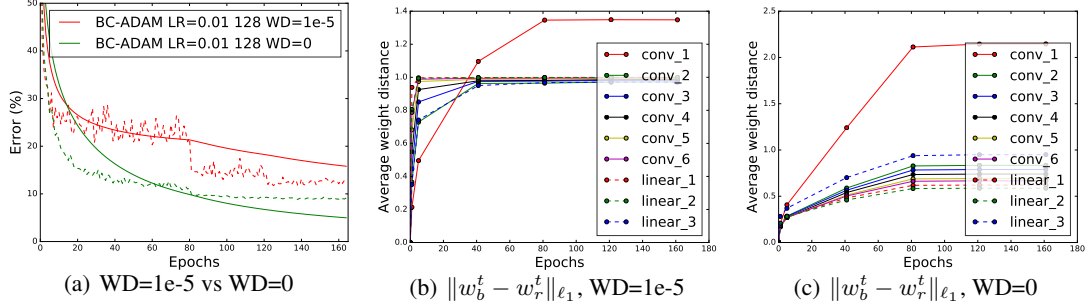


Figure 6: The effect of weight decay (WD) on BC-ADAM. The y-axis of (b) and (c) is the averaged weight difference between the binary weights w_b and the real-valued weights w_r , i.e., $\frac{1}{d} \|w_b^t - w_r^t\|_1$. where d is the number of weights in w_b .

H.4 Weight Decay

Figure 6 shows the effect of applying weight decay to BC-ADAM. As shown in Figure 6(a), BC-ADAM with 1e-5 weight decay yields worse performance compared to zero weight decay. Applying weight decay in BC-ADAM will shrink w_r to 0, as well as increase the distance between w_b and w_r . Figure 6(b) and 6(c) shows the distance between w_b and w_r during training. With 1e-5 weight decay, the average weight difference between w_b and w_r approaches to 1, which indicates w_r is close to zero. Weight decay cannot “decay” the weight of SR as $\|w_b\|_2$ is the same for all binarized networks.